Article | Received 9 October 2025; Revised 16 November 2025; Accepted 28 November 2025; Published 28 November 2025
https://doi.org/10.55092/sc20250029

XGBoost-based intelligent framework for asphalt pavement skid resistance assessment under different variables

Yu Zhao[1], Mohd Rosli Mohd Hasan[1,*], Ke Zhang[2], Lingyun You[3], Ali Jamshidi[1,4] and Junxian Jiang[5]

[1] School of Civil Engineering, Universiti Sains Malaysia (Engineering Campus), Nibong Tebal 14300, Malaysia
[2] School of Business, Fuyang Normal University, Fuyang 236041, China
[3] School of Civil and Hydraulic Engineering, Huazhong University of Science and Technology, Wuhan 430074, China
[4] School of Science, Technology and Engineering, University of the Sunshine Coast, Sippy Downs 4556, Australia
[5] School of Housing, Building and Planning, Universiti Sains Malaysia, Nibong Tebal 11800, Malaysia

* Correspondence author; E-mail: cerosli@usm.my.

Highlights:

- XGBoost-based intelligent framework was used to model asphalt pavement skid resistance.
- Multi scale integrated texture statistics and fractal feature characterization were adopted.
- The result indicates that AC13 dense graded mixtures demonstrate the highest prediction accuracy.
- Fractal dimension is the core predictive factor with the highest feature importance, and gradation types significantly influence the effectiveness of features.
- The aggregate gradation-adaptive anti-skidding evaluation, supported by feature importance analysis.

Abstract: To address the constraints of conventional evaluation methods for asphalt pavement anti-skidding performance, such as insufficient generalization across gradation scenarios and difficulties in collaborative quantification of multi-scale features, this study proposes a composite parameter-based asphalt pavement anti-skidding performance evaluation model using the XGBoost algorithm. The study selected three typical types of asphalt pavements, AC13, AC20, and SMA13, which are widely used in paving practice. The texture feature information of these test road sections was extracted and developed a full-scale texture characterization system by integrating the statistical features (energy and entropy) and fractal features (fractal dimension and multifractal spectrum width Δα). The feature segmentation counting method was employed to quantify the contribution mechanism of different texture features to skid resistance, and the application effectiveness of the model in cross-gradation scenarios was systematically evaluated. The results showed that XGBoost-based composite parameter asphalt pavement anti-skidding performance evaluation model achieved test set accuracy of $R^2 > 0.9$ and RMSE < 0.06, confirming its capability to accurately and effectively assess asphalt pavement anti-skidding

performance. Model performance was influenced by pavement gradation type: AC13 fine-graded mixtures yielded optimal prediction, SMA13 mixtures ranked second, while AC20 coarse-graded mixtures exhibited relatively weaker generalization but still met requirements. Feature importance analysis identified fractal dimension as the core predictive factor of the model, with different gradation types significantly affecting the effectiveness of texture feature characterization. The research provides significant theoretical and technical support for achieving intelligent detection and gradation-adaptive evaluation of asphalt pavement anti-skidding performance.

Keywords: asphalt pavement; anti-skidding performance; texture features; gradation types; image analysis; artificial intelligence

1. Introduction

The anti-skidding performance of asphalt pavement refers to its ability to resist slippage caused by wheel abrasion during service. This performance significantly impacts pavement durability and service life while being critically linked to road traffic safety [1–3]. As a key indicator for post-construction maintenance, repair, and acceptance of highways, anti-skidding performance directly influences road quality assessment, condition evaluation, maintenance scheduling, and strategy selection [4,5].

The anti-skidding performance primarily depends on the friction between vehicle tires and the pavement surface, ensuring safe acceleration, deceleration, and braking operations [6]. Pavement texture characteristics substantially govern the magnitude of tire-pavement friction, thereby determining anti-skidding performance [7–9]. Among these characteristics, macro texture and micro texture primarily govern the skid resistance of asphalt pavements [2,10]. Macro texture typically manifests as larger-scale irregular surface features on asphalt pavement, which are related to the spacing between aggregate particles [11,12]. Micro texture refers to smaller-scale irregularities (micron-level roughness) on aggregate surfaces, primarily determined by the surface texture of hardened binders and aggregates [13,14]. Generalized friction theory successfully separates macro texture and micro texture contributions, establishing a foundation for multiscale mechanistic analysis [15]. The Pearson correlation coefficient provides an effective measure for quantifying how texture parameters influence anti-skidding performance [16]. Furthermore, the pavement texture characteristics of asphalt surfaces at different scales exhibit distinct functional differences, particularly significantly influencing skid resistance, playing a decisive role in the overall pavement safety performance [11,17]. Fractal theory further correlates micro texture morphology of coarse aggregate surfaces with anti-skidding performance, guiding the practical application of aggregates with higher fractal dimensions in pavement surface layers to enhance skid resistance [18].

Current evaluation of asphalt pavement anti-skidding performance primarily considers friction coefficient and texture depth, categorized into contact and non-contact measurement techniques based on instrumentation principles [1,19]. Contact-based measurement refers to fixed-point testing using traditional equipment, including Sand patch method, Pendulum friction tester method, Dynamic rotational friction coefficient tester method. These methods indirectly evaluate pavement surface texture characteristics through instrument-measured indicators or calculated parameters, thereby assessing pavement anti-skidding performance [20]. Full-scale track testing using the contact-based methods reveals that different testing conditions and methodologies significantly influence anti-skidding

performance indicators [21]. Due to the limitations of contact-based measurement methods, numerous researchers have extensively investigated non-contact measurement approaches. Current mainstream non-contact measurement techniques include close-range photogrammetry, digital grayscale imaging, and laser measurement [22]. These methods primarily utilize multi-form sensors to scan specific pavement areas, extract morphological feature parameters, and calculate texture characteristics to evaluate anti-skidding performance [1]. Among them, the texture information of asphalt mixture can be extracted through binocular stereo vision, and high-precision 3D pavement morphology can be reconstructed using digital image processing, thereby constructing a predictive mapping between texture features and anti-skidding performance [23,24].

Although previous studies have multi-dimensionally validated the correlation mechanisms between the textural characteristics of asphalt pavements and their skid resistance, traditional evaluation methods cannot collaboratively quantify the nonlinear coupling effects of multi-scale texture features on friction force, lack intelligent transformation models converting texture features to anti-skidding performance, and exhibit significant degradation in generalization capability across gradation scenarios, failing to analyze texture-friction relationship variations caused by material structural differences. The XGBoost algorithm, as an emerging machine learning method, incorporates prior knowledge, streamlines network architecture, establishes explicit hierarchies, ensures robust feature representation in model outputs, and enhances computational efficiency and training speed [25–27]. Compared to other machine learning algorithms, this model demonstrates superior accuracy, stability, and robustness [28]. Therefore, this study proposes constructing a composite parameter-based anti-skidding evaluation model using the XGBoost algorithm. By integrating statistical and fractal features of asphalt pavement textures into a full-scale characterization system, leveraging XGBoost algorithm regularization constraints and second-order gradient optimization mechanisms to resolve fitting conflicts between high-dimensional features and small-sample data, and implementing gradation-adaptive evaluation through feature importance analysis, the study makes significant contributions toward intelligent assessment of asphalt pavement anti-skidding performance. The overall technical framework implementing this research is illustrated in Figure 1.

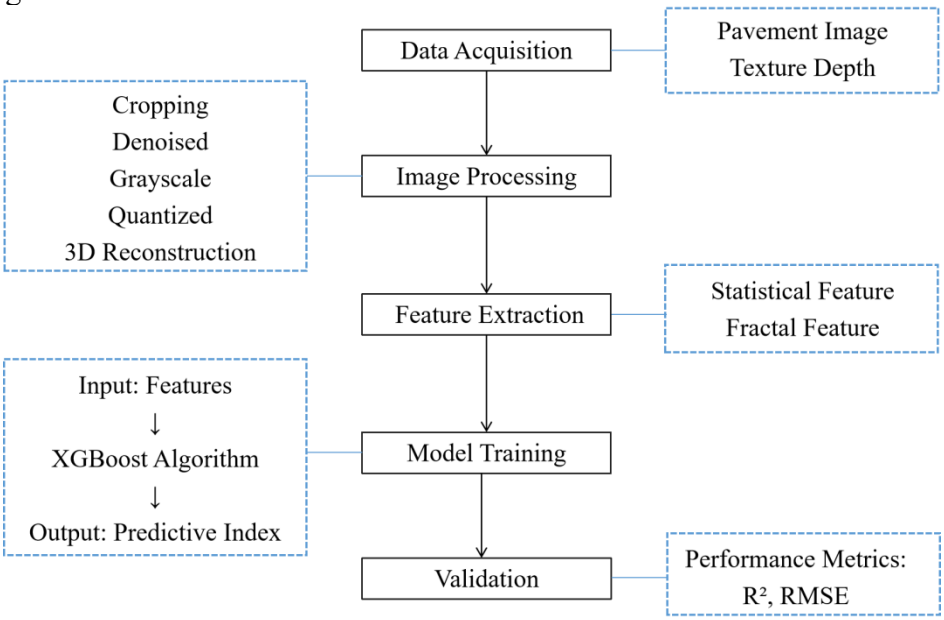

Figure 1. Research framework for the study.

2. Research methodology

2.1. Data collections via field measurement

This study selected the Shi-Wu Expressway in Hubei Province, China, for pavement texture and texture depth data collection. Through comprehensive review of the entire route's design data combined with on-site investigations, with full consideration of different engineering sections, diverse road segment types, differentiated structural designs, and geographical environmental conditions, 18 representative typical field test sections were selected.

As shown in Figure 2, each test section spans 1000 meters in length. At the starting point of each selected test section, four initial measurement points were defined on the transverse section: located at the middle of the right-side first traffic lane (fast lane) (Point 1), middle of the right-side third traffic lane (slow lane/emergency lane) (Point 2), middle of the left-side third traffic lane (slow lane/emergency lane) (Point 3), and middle of the left-side first traffic lane (fast lane) (Point 4). Subsequently, along the driving direction, subsequent measurement points were longitudinally arranged at 40-meter equidistant intervals, specifically establishing four corresponding transverse measurement points at 40 meters longitudinally from the initial four points, with this pattern repeated throughout the section. Following this methodology of deploying four transverse measurement points per longitudinal position, a total of 100 measurement points were established along the 1000-meter section.

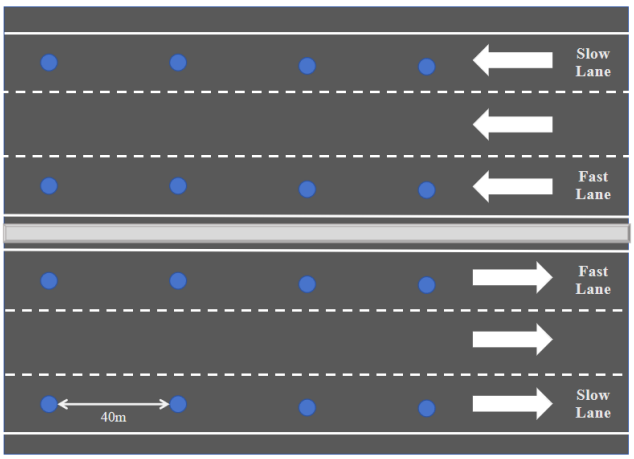

Figure 2. Schematic diagram of on-site measurement location.

To ensure sufficient regional representativeness and technical coverage, the 18 selected field test sections encompassed three typical asphalt mixture gradation types widely used in engineering practice: AC13, AC20, and SMA13, with each gradation type containing six independent test sections. This sampling strategy ensured the inclusion of significant variability in pavement characteristics resulting from different gradations, lane positions, and road sections within the single regional expressway, thereby enhancing the representativeness of the dataset and the robustness of the developed model.

To establish a reliable methodology under ideal baseline conditions, all tests were conducted on dry and clean pavement surfaces to ensure good consistency and repeatability, as shown in Figure 3. Firstly, a self-developed pavement texture acquisition device was utilized to capture pavement texture images at each measurement point. The device underwent multiple rounds of environmental simulation and field debugging optimization, with its final critical acquisition parameters (e.g., frame height, shading

mechanism, light source intensity and height) summarized in Table 1. Under strict adherence to configured parameters, standardized image acquisition of asphalt pavement textures could be performed. Subsequently, at corresponding areas of the same measurement point, the sand patch method was immediately employed for the determination of texture depth (TD).

(a) (b)

Figure 3. Process of data collection. **(a)** Mobile setup for image recording; **(b)** Texture depth measurement.

Table 1. Setting parameter for pavement texture collection device.

Parameter Category	Parameter Name	Setting Value	Remarks
Camera Parameters	CCD Resolution	20 megapixels	Ensures clear texture details
	Aperture	f/8	Balances depth of field and light intake
	Shutter Speed	1/125 s	Matches device stability requirements
Light Source Parameters	LED Brightness	3000 lm (lumens)	Avoid image overexposure or shadows
	LED Quantity	4 groups (symmetrical distribution)	Eliminates texture shadows caused by unilateral lighting
	Color Temperature	5500 K (daylight white balance)	Reduces color deviation
	Light Source Angle	45° (angle with pavement surface)	Enhances contrast between convex/concave textures
Other Parameters	Light Source Height	50 cm	Ensures complete illumination coverage
	Shooting Height Adjustment Pole	80 cm	Guarantees full coverage of image acquisition area
	Shade Hood Angle/Length	Full coverage	Blocks ambient stray light interference
	Shooting Angle	Vertical downward (90°)	Reduces image distortion via orthogonal projection
	Sampling Interval	≥ 20 m (along pavement longitudinal direction)	Ensures validity of collected data

2.2. Data processing

Accurate extraction of texture features from asphalt pavement images is a critical prerequisite for evaluating anti-skidding performance [29]. First, the acquired asphalt pavement texture images are converted into 256-level grayscale images. As shown in Figure 4, MATLAB R2018b can be used to preprocess the acquired images, including image cropping, noise reduction. Due to common issues such as uneven illumination or sensor noise in asphalt images, and to mitigate the risks of overexposure (high grayscale values) or underexposure (low grayscale values), grayscale quantization was applied to smooth minor grayscale fluctuations and highlight macroscopic texture structures [30]. A Gray-level Co-occurrence Matrix (GLCM) was constructed from images whose grayscale had been discretized into 8 levels. Due to the dependence of GLCM calculations on pixel distribution and grayscale resolution, excessive grayscale levels or large pixel values could lead to increased computational complexity and processing time [31]. To address this, practical parameter settings were adopted: pixel spacing was uniformly set to 1, and four angles (0°, 45°, 90°, and 135°) were selected for GLCM computation to balance accuracy and efficiency.

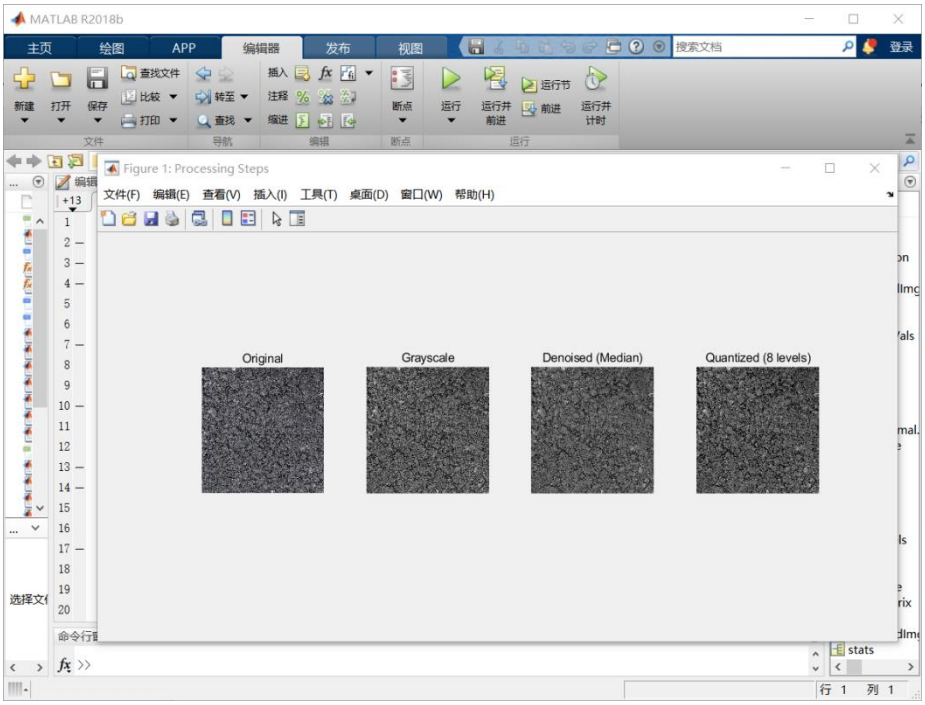

Figure 4. Screenshot of process for pavement texture images processing using MATLAB R2018b.

In the 3D reconstruction of pavement texture images, the Shape from Shading principle is applied to reconstruct the 3D morphology from 2D images using specific algorithms [23,32]. During image acquisition with the designed device, diffuse reflection occurs due to surface irregularities, manifesting as grayscale variations in pixels that correspond to concave and convex features on the pavement surface. To restore the 3D morphology, a proportional weight adjustment method is used to calibrate the relationship between grayscale values and measured TD. As illustrated in Figure 5, the acquired pavement texture images undergo preprocessing steps, including image cropping, grayscale conversion, and median filtering for noise reduction, followed by the aforementioned 3D reconstruction process. Using

MATLAB R2018b, the analysis of spatial coordinates and grayscale data extracted from preprocessed images enabled the construction of a three-dimensional texture model, as visualized in Figure 6.

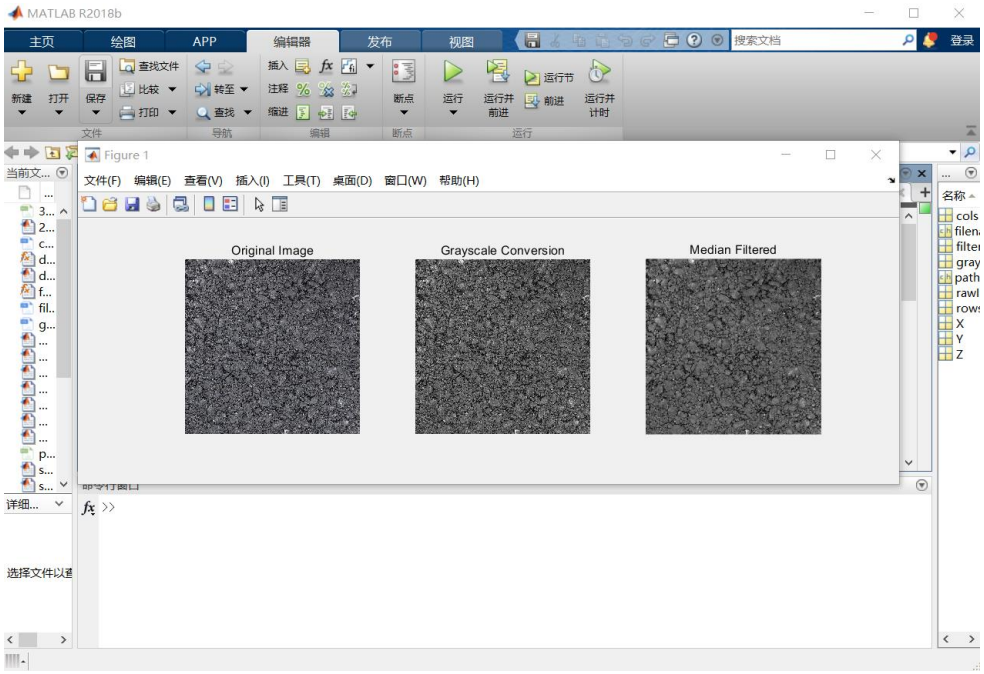

Figure 5. Screenshot of process for 3D reconstruction of pavement texture using MATLAB R2018b.

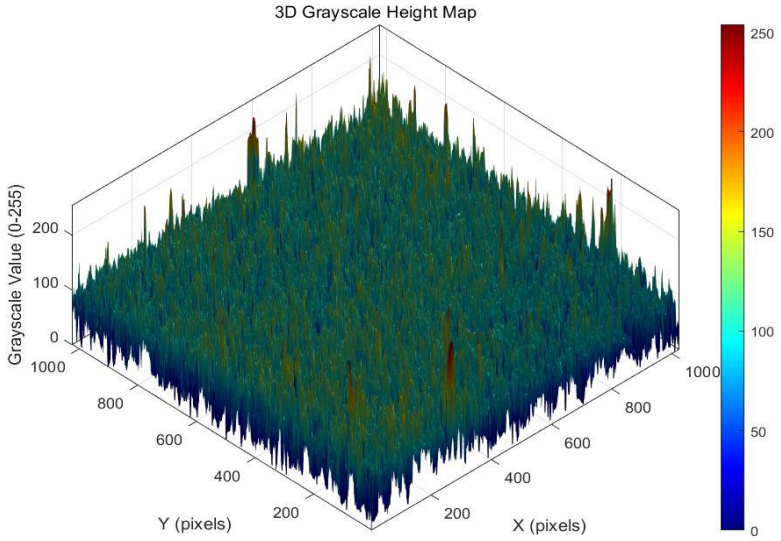

Figure 6. 3D reconstruction of pavement texture image.

2.3. Pavement texture feature parameters

2.3.1. Statistical characteristics

Statistical characteristics refer to texture features evaluated through statistical methods, which quantify morphological attributes of pavement surfaces, including height distribution, curvature, and geometric shape. These characteristics critically influence the tire-pavement contact mechanics and drainage

efficiency, thereby directly affecting the skid resistance performance of the pavement surface [33]. Given the intricate and diversity of asphalt pavement texture information, it is necessary to conduct a rigorous and comprehensive analysis and evaluation of texture characteristics. A widely adopted method for texture feature analysis is the GLCM, introduced by Haralick *et al*. in the 1970s, which offers a robust statistical framework for quantifying image texture [34,35]. This technique represents texture by statistically quantifying the spatial relationships between pairs of pixels with specific gray-level intensities within a defined spatial domain [36]. Among the statistical measures derived from the GLCM, this study selected energy and entropy as statistical feature parameters to analyze different image texture features. These parameters were chosen for their ability to cover the primary dimensions of texture analysis and their high discriminative power in texture classification and feature extraction.

Energy, also known as the angular second moment, is calculated as the sum of squared values of all elements within the GLCM. This measure indicates the uniformity of gray-level distribution and the textural coarseness in an image. In the analysis of asphalt pavement anti-skidding performance, a more uniform surface texture corresponds to GLCM elements that are similar in value, which yields a lower energy measure [30]. Conversely, when the pavement texture is rough, the values of the co-occurrence matrix in different directions differ significantly, leading to higher energy in the image. Equation (1) shows the formula to determine the energy value for characterizing asphalt pavement texture:

$$Energy = \sum_{i=1}^{N} \sum_{j=1}^{N} \left[P(i, j) \right]^2 \tag{1}$$

Here:

^{i,j}: Row and column indices of the GLCM, representing the gray-level values of two pixels (e.g., i for the reference pixel, j for the neighboring pixel).

^{N}: Total number of gray levels in the image (e.g., 256 levels for 8-bit images, often reduced to 8 levels for computational efficiency).

$^{P(i,j)}$: Normalized GLCM element, representing the joint probability of gray-level pairs i and j occurring at a specific direction and distance.

Entropy quantifies the degree of randomness in the information present within an image, serving as an indicator of the irregularity inherent in its content. This measure reflects the complexity of the gray-level distribution across the image: greater entropy corresponds to higher complexity [37]. In evaluating asphalt pavement anti-skidding performance, the entropy value extracted from digital images can describe the textural intricacy of the pavement surface. Smoother textures observed in pre-captured images result in lower entropy, whereas more irregular textures lead to elevated entropy values. Equation (2) provides the computational formula for entropy applied to characterize asphalt pavement texture:

$$Entropy = -\sum_{i=1}^{N} \sum_{j=1}^{N} P(i, j) \cdot \log_2 P(i, j) \tag{2}$$

Here:

$^{i,j,\ N,\ P(i,j)}$: Same as above.

2.3.2. Fractal characteristics

Fractal geometry has been popular for many years in image analysis and texture recognition due to its excellent performance and applications, particularly in analyzing pavement texture roughness [38]. The anti-skidding performance of asphalt pavement is governed by a wide array of complex factors. These factors can be understood as exhibiting randomness and statistical self-similarity within certain ranges, characteristics that are often difficult to describe accurately using conventional mathematical language [39]. Fractal theory, as a novel theoretical tool for studying irregular phenomena in nature, is applicable to describing and evaluating objects with statistical self-similarity [40,41]. Since the microscopic morphology of pavement surfaces exhibits self-similarity, it is feasible to use fractal theory to characterize pavement textures.

Currently, the differential box-counting method is widely recognized for its computational stability, algorithmic simplicity, and implementation efficiency among fractal dimension calculation approaches [42]. The calculation process of this method is as follows:

An M × M grid representing the vertical projection of a three-dimensional surface is partitioned into smaller subgrids of size s (where $M/2 \geq s \geq 2$, with s being an integer). The scale ratio is defined as r = s/M. In this framework, the x- and y-axes correspond to spatial coordinates, while the z-axis denotes height (or grayscale intensity). Each s × s subgrid is examined using a series of volumetric units of size s × s × h, where h represents the box height, set as h = s/M.

Within any given (x,y) subgrid, let the minimum and maximum surface heights fall into the k-th and l-th boxes, respectively. The number of boxes needed to cover the surface within the subgrid is:

$$n_r(i,j) = l - k + 1 \tag{3}$$

Here, *nr(i,j)* denotes the box count covering the surface in the (i, j)-th subgrid.

The total number of boxes required to cover the entire surface is obtained by summing over all subgrids:

$$N(r) = \sum_{i,j} n_r(i,j) \tag{4}$$

The fractal dimension D is then defined as:

$$D = \lim_{r \to 0} \frac{\ln N(r)}{\ln(1/r)} \tag{5}$$

In the context of asphalt pavement 3D texture analysis, the surface is systematically covered using cubic boxes of side length r. The number N(r) of boxes that intersect the surface is tallied for varying r values. A log-log plot of lnN(r) against ln(1/r) is constructed, and the fractal dimension is derived from the slope of the linear fit applied to the data points (ln(1/r), lnN(r)) via least squares regression.

$$\ln N(r) = D \ln(1/r) + b \tag{6}$$

To capture more comprehensive and refined pavement morphology information, multifractal theory can be employed to describe the probability distribution of fractal geometries across hierarchical levels. This approach divides complex fractal structures into multiple regions for analysis, thereby characterizing the inhomogeneity of the study object and addressing the limitations of simple fractal

dimensions [43]. Within this framework, the multifractal spectrum α-f(α) provides a quantitative description of the heterogeneity, irregularity, and complexity of the fractal system. By considering the binarized image as a measure space, the analyzed domain is divided into N subregions. For the i-th subregion with scale εi, the probability measure Pi is characterized by a scaling exponent αi. The relationship between Pi and εi is expressed as Equation (7):

$$P_i(\varepsilon_i) = \varepsilon_i^{\alpha_i} \tag{7}$$

The partition function is defined as Equation (8):

$$\chi(q,\varepsilon) = \sum_i P_i^q \tag{8}$$

Here:

q: the order parameter, which theoretically spans from negative to positive infinity but is typically limited to $-100 \le q \le 100$.

Asphalt pavement surface morphology exhibits strong multifractal characteristics, demonstrating a robust linear relationship in the scaling analysis [42]. To enhance computational efficiency, as shown in Equation (9), the approach introduced by Chhabra et al. is commonly used to orthogonalize the probability measure.

$$u_i(q,\varepsilon) = \frac{P_i^q(\varepsilon)}{\sum_{i=1}^{N(\varepsilon)} P_i^q(\varepsilon)} \tag{9}$$

Then calculate the multifractal spectrum according to Equations (10) and (11):

$$\alpha(q) = \lim_{\varepsilon \to 0} \frac{\sum_{i=1}^{N(\varepsilon)} u_i(q,\varepsilon) \ln P(\varepsilon)}{\ln \varepsilon} \tag{10}$$

$$f(q) = \lim_{\varepsilon \to 0} \frac{\sum_{i=1}^{N(\varepsilon)} u_i(q,\varepsilon) \ln u_i(q,\varepsilon)}{\ln \varepsilon} \tag{11}$$

The multifractal spectrum, which describes the 3D morphology of the pavement surface, is obtained by plotting α(q) against f(q) in α-f(α) coordinates. Key multifractal parameters include the spectrum width Δα and the spectrum difference Δf, as defined in Equations (12) and (13):

$$\Delta\alpha = \alpha_{\max} - \alpha_{\min} \tag{12}$$

$$\Delta f = f(\alpha_{\min}) - f(\alpha_{\max}) \tag{13}$$

Here:

$\Delta\alpha$: quantifies the heterogeneity of the probability measure distribution across all fractal structures.

Δf : represents the proportion of quantities contained in subsets with the maximum and minimum probabilities.

Among them, the multifractal parameter spectral width Δα can reflect the overall variation range of singularity in texture distribution, with larger values indicating more pronounced variations in pavement texture. The multifractal parameter spectral difference Δf describes the dimension difference at both ends of the multifractal spectrum, which only characterizes the distribution quantity contrast between the densest and sparsest regions in the texture, and thus fails to comprehensively describe the aggregation-dispersion characteristics of the texture [42]. Therefore, the Multifractal spectral width Δα is selected as the principal parameter for characterizing the multifractal features of pavement texture.

3. Evaluation model for anti-skidding performance of asphalt pavement based on XGBoost algorithm

3.1. Principle of XGBoost model

Decision tree is a tree-structured machine learning model that constructs a predictive tree structure through feature recursive splitting, with data features as nodes, feature values as branches, and decision outcomes as leaf nodes. Its core objective is to maximize within-subset homogeneity and between-subset heterogeneity [44,45]. Ensemble learning represents a broad category of model fusion strategies that combine predictions from multiple base learners (e.g., decision trees) to enhance overall predictive performance, with its general structure illustrated in Figure 7. Typically, a single decision tree model exhibits limited predictive capability and practical applicability. By combining multiple learners, ensemble learning achieves superior generalization performance compared to individual learners, thereby enhancing the application value of the model [46,47]. Based on the method of generating individual learners, current ensemble learning approaches are primarily categorized into two major types: boosting and bagging. Boosting employs a sequential training process that assigns higher weights to samples misclassified by the preceding base learner, making each training iteration dependent on previous results [48,49]. The final decision outcome is obtained through weighted summation of outputs from multiple base learners. To overcome the generalization limitations of single decision trees, this study adopts the representative algorithm XGBoost (Extreme Gradient Boosting) as an enhanced version of Gradient Boosted Decision Trees, which integrates multiple base learners to improve predictive performance [50]. Its core computational principles are depicted in Figure 8.

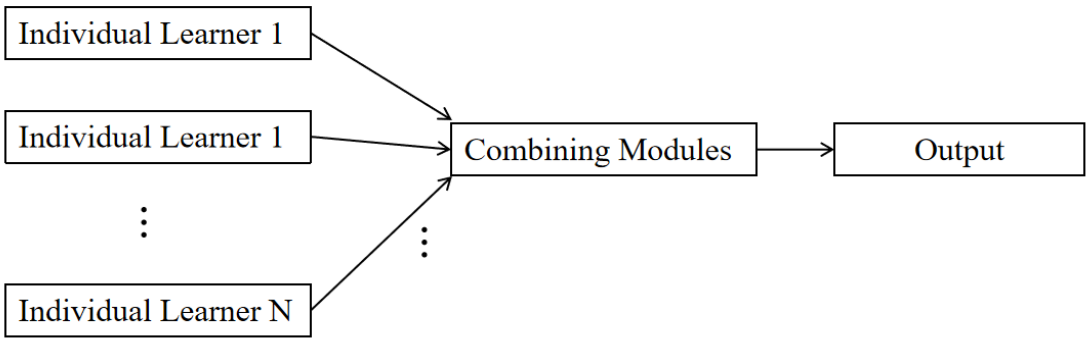

Figure 7. Integrated learning diagram.

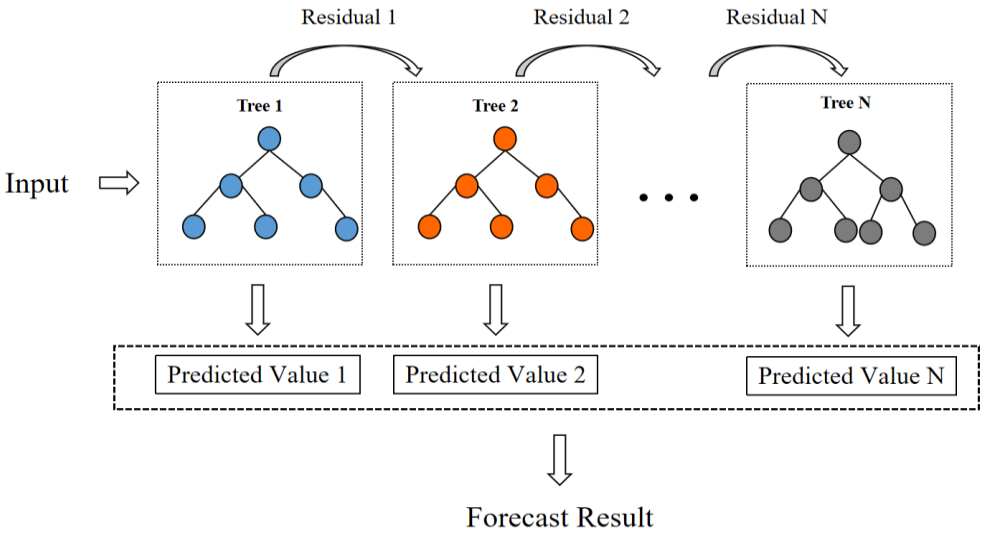

Figure 8. Core computing schematic diagram.

The core principles of the XGBoost model include loss function, regularization term, objective function and model update [48]. By leveraging first-order and second-order derivative information, the XGBoost model can more accurately estimate the loss for each sample, thereby enhancing prediction accuracy. The regularization prevents overfitting by constraining model complexity. Additionally, XGBoost applies pruning techniques to reduce tree size, further lowering model complexity and improving generalization capability. The model's support for custom loss functions and evaluation metrics enables adaptability to diverse tasks and requirements, while also facilitating feature selection and model interpretation.

3.2. Development of evaluation models for anti-skidding performance

Based on the texture characteristics characterized by energy and entropy derived from the GLCM, fractal dimension, and multifractal spectrum width $\Delta\alpha$, these parameters were designated as feature values, while texture depth (TD) served as the label data to construct a dataset comprising 1,800 sets of data. The dataset was split randomly into a training set (70%) and an evaluation set (30%), with a composite parameter-based asphalt pavement skid resistance evaluation model established using the XGBoost algorithm.

The model employs a gradient-boosted tree framework. Due to the numerous adjustable parameters of the algorithms, a two-layer grid search strategy was implemented to optimize hyper-parameters, enhancing skid resistance evaluation performance while improving learning efficiency. During the first stage, coarse-grained search identified parameter ranges; the second stage then performed fine-grained optimization, dynamically adjusting parameter step sizes within optimal neighborhoods. As detailed in Table 2, critical hyper-parameters include a learning rate of 0.2, maximum tree depth of 4, subsample rate of 0.61, column sample rate of 0.64, and 120 iterations, achieving balance between model complexity and the deviation-variance trade-off. Training incorporated early stopping and 5-fold cross-validation, with gradient optimization realized through dynamic tree-weight adjustments.

Table 2. XGBoost model: hyper-parameter setting.

Hyper-parameter Name	Set Value/Range	Function Description
Learning Rate	0.2	Shrinks the contribution of each tree; lower values require more trees but improve stability.
Max Tree Depth	4	Controls the maximum depth of individual trees; higher values may lead to overfitting.
Number of weak learners	120	Total number of base models (trees) in XGBoost; affects model complexity and training time.
L1 regularization weight	Not specified (default = 0)	Controls L1 regularization strength (reg_alpha) for feature selection.
L2 regularization weight	Not specified (default = 1)	Controls L2 regularization strength (reg_lambda) to prevent overfitting.

To assess the stability of the established model and reduce the randomness associated with a single random split, an additional multi-run validation procedure was performed after the final hyper-parameters were determined. The entire dataset of 1800 samples were randomly partitioned into five mutually exclusive subsets. Iteratively, one subset was used as the testing set while the remaining four served as the training set, and this process was repeated five times. The mean and standard deviation of the performance metrics from the five runs were calculated to provide a robust estimate of the model's performance. The results of this multi-run validation are presented in Table 3, demonstrating the high stability and reliability of the model.

Table 3. Performance stability assessment of the model across multiple validation runs.

Metric	Value (Mean ± Standard Deviation)
R^2	0.903 ± 0.009
RMSE	0.048 ± 0.006

4. Results and discussion

4.1. Model accuracy and result analysis

Three different gradation types (AC13, AC20, and SMA13) of asphalt pavement anti-skidding performance evaluation parameters were calculated based on the XGboost model. The texture depth (TD) at relevant locations was determined through the sand patch method. To gauge the performance of the machine learning models, the coefficient of determination (R^2) and root mean square error (RMSE) were adopted as evaluation measures [51–53]. Among them, R^2 measures the goodness of fit of a model to the observed data, with values ranging from 0 to 1. RMSE quantifies prediction accuracy by computing the square root of the average squared deviations between estimated and measured values. Based on these criteria, the composite parameter-based asphalt pavement skid resistance evaluation model established in the study was systematically evaluated. Figure 9 presents the training and testing results of this model.

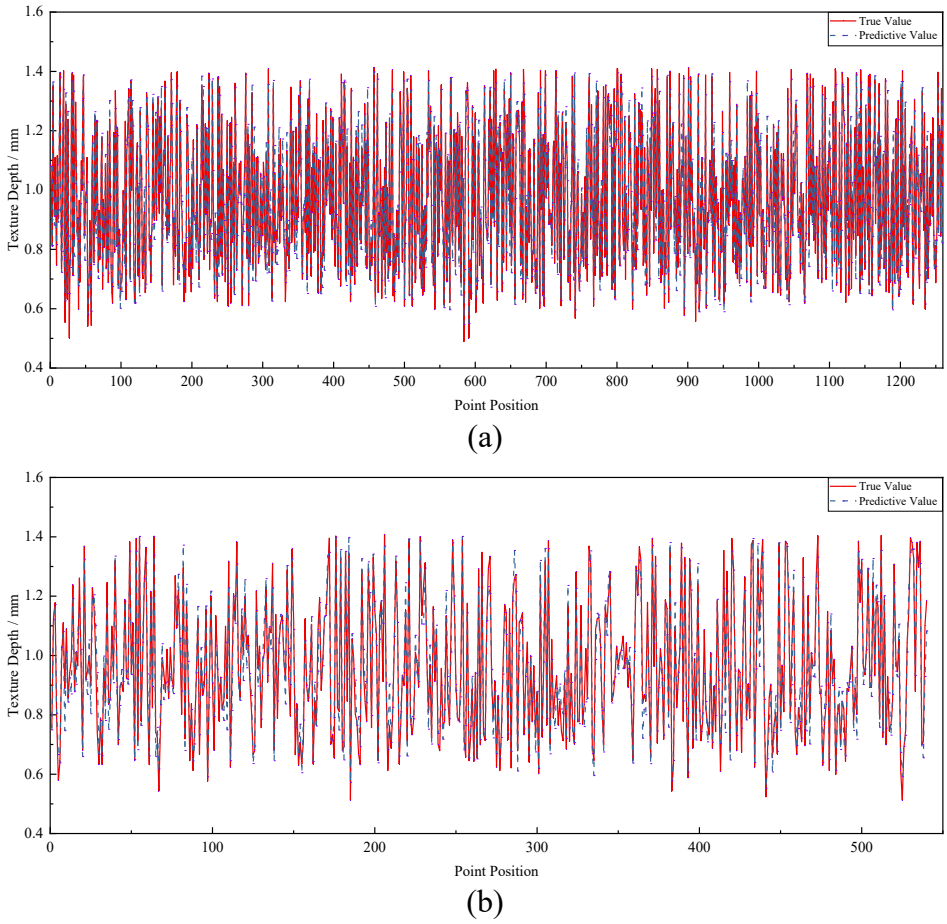

Figure 9. Testing and training results of the XGboost model. **(a)** testing set; **(b)** training set.

As shown in Figures 10 and 11, the composite parameter-based asphalt pavement skid resistance evaluation model constructed using the XGBoost algorithm exhibited excellent predictive capabilities. The determination coefficient ($R^2 > 0.9$) and root mean square error (RMSE < 0.1) for the training set indicate that the model has excellent fitting effect on the training data and can fully capture the nonlinear relationship between input features (energy, entropy, fractal dimension, and multifractal spectrum width $\Delta\alpha$) and texture depth (TD), achieving high-precision learning. Meanwhile, the determination coefficient ($R^2 > 0.9$) and root mean square error (RMSE < 0.1) of the testing set further validated the strong generalization performance of the model on unseen data. Notably, the R^2 difference between the testing set and the training set is extremely small, indicating that the model has not shown significant overfitting and has good structural robustness. In terms of prediction accuracy, with the R^2 exceeding 0.9 for the testing set, the model explained over 90% of texture depth variability, surpassing the accuracy of conventional pavement performance prediction models (typically $R^2 < 0.85$). Combined with RMSE results, the prediction error of the model is at a sufficiently low level, which can meet the accuracy requirements for quantitative evaluation of anti-skidding performance in pavement engineering.

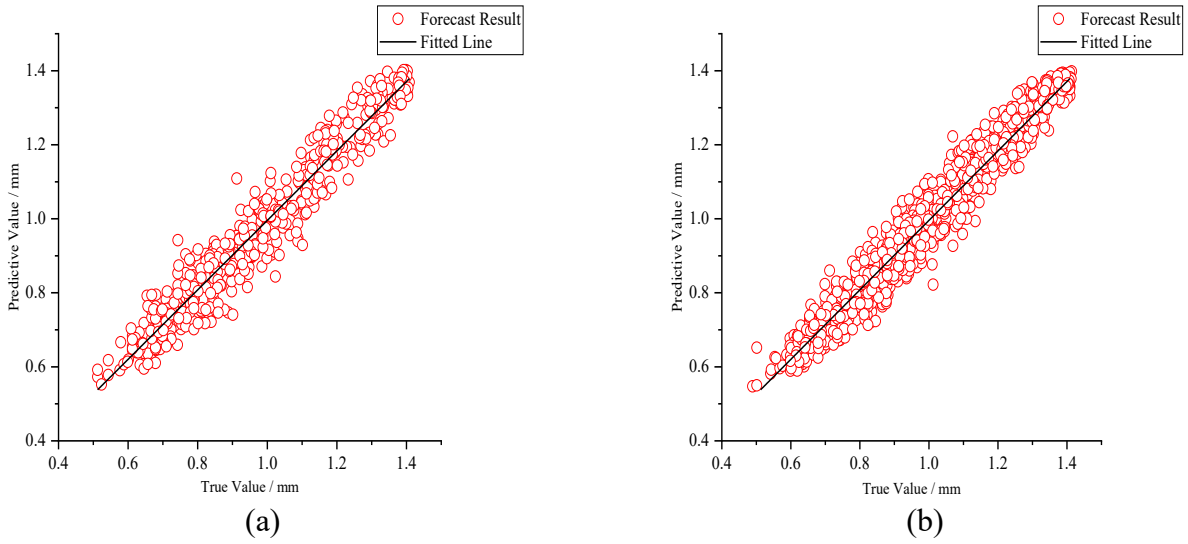

Figure 10. Relationship between true value and predictive value. **(a)** testing set; **(b)** training set.

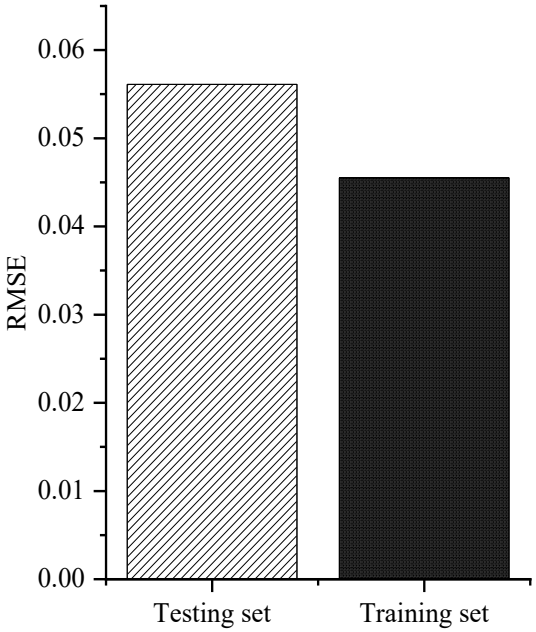

Figure 11. Root Mean Square Error (RMSE) results of the model.

4.2. Comparison and analysis of XGBoost model performance with various gradation types

In order to further investigate the effectiveness of the XGBoost algorithm-based asphalt pavement skid resistance evaluation model in assessing different gradation types, analyses and comparisons were conducted on datasets collected from three typical asphalt pavement gradations (AC13, AC20, and SMA13). Figures 12 and 13 respectively display the training and testing results of models based on these three gradation types.

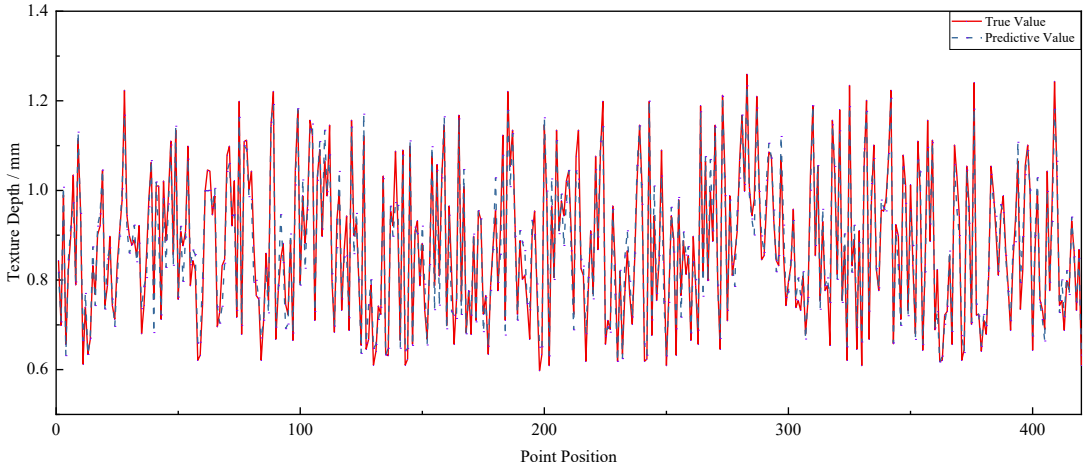

(a)

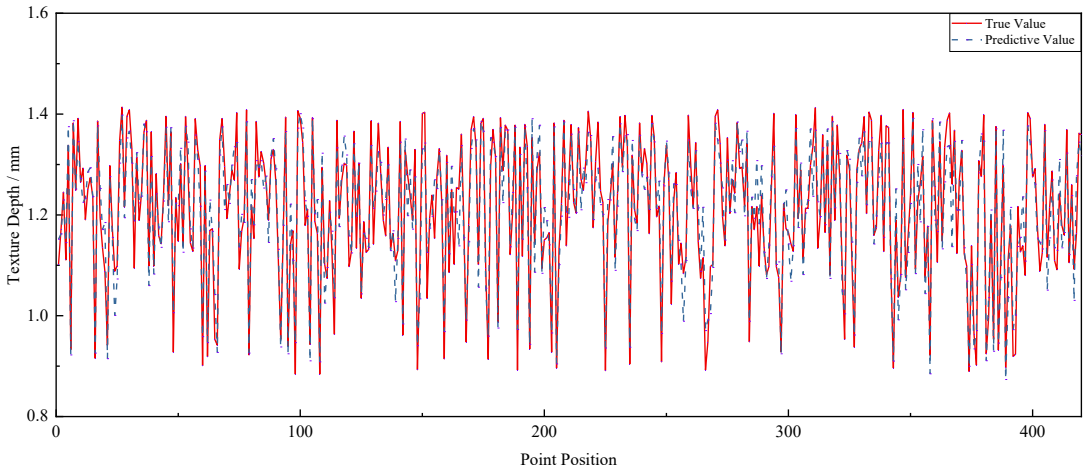

(b)

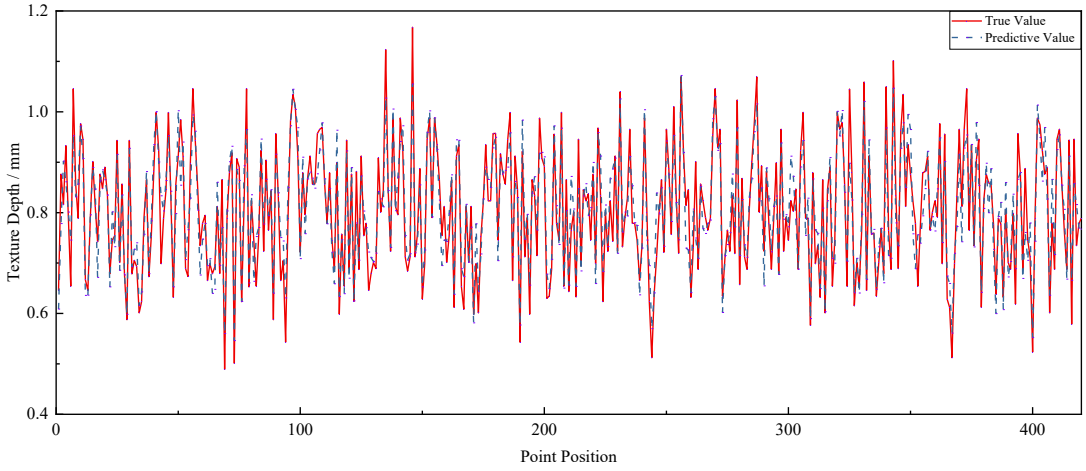

(c)

Figure 12. Model training results of asphalt pavement with different gradation types. **(a)** AC13; **(b)** SMA13; **(c)** AC20.

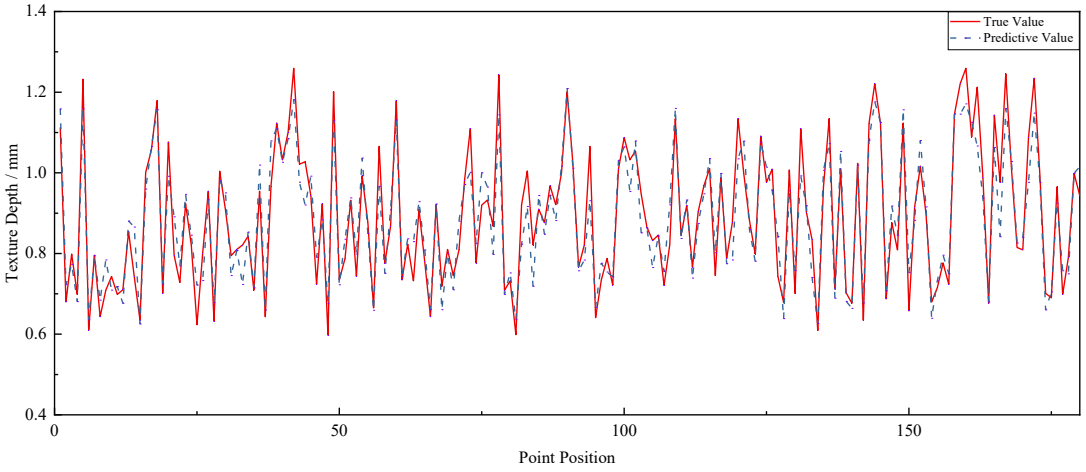

(a)

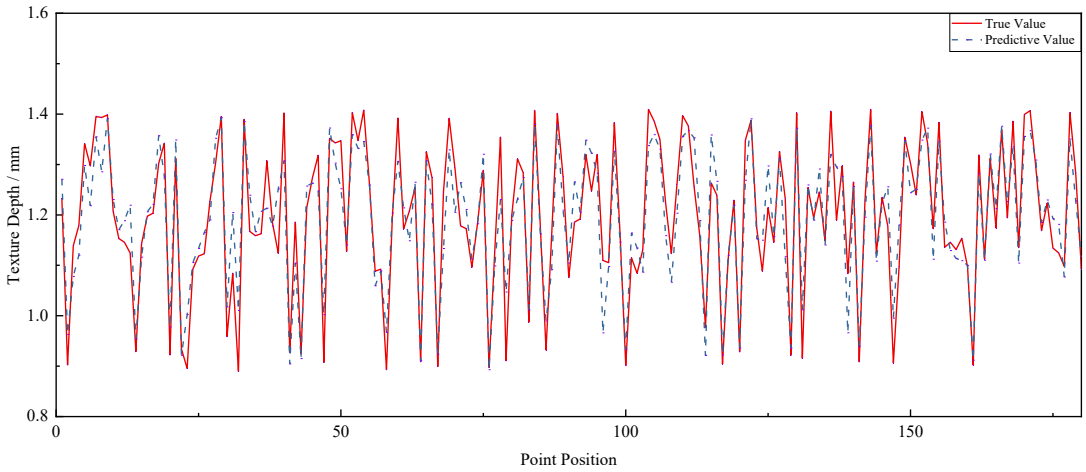

(b)

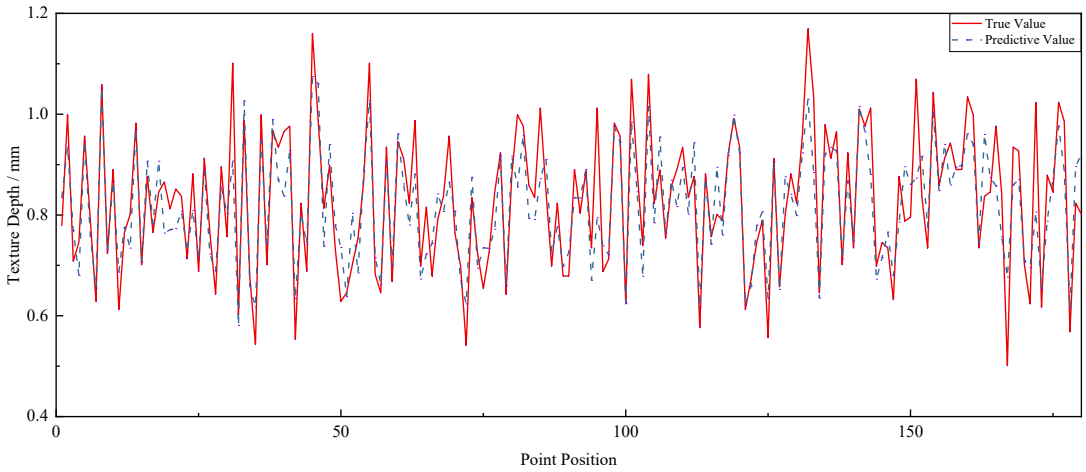

(c)

Figure 13. Model testing results of asphalt pavement with different gradation types. **(a)** AC13; **(b)** SMA13; **(c)** AC20.

As indicated by the results in Figure 14, the performance of the model exhibited significant variations when evaluating asphalt pavements with different gradation types. Among them, the asphalt pavement with AC13 gradation achieved optimal prediction accuracy (R^2 = 0.925, RMSE = 0.045),

followed by SMA13 gradation (R^2 = 0.885, RMSE = 0.049), while the asphalt pavement with AC20 gradation demonstrated relatively weaker generalization capability (R^2 = 0.816, RMSE = 0.056). This gradient-like discrepancy primarily originates from differences in the adaptability of surface texture characteristics among distinct gradation materials to feature characterization, revealing variations in the difficulty of characterizing aggregate size distribution and pavement surface texture features.

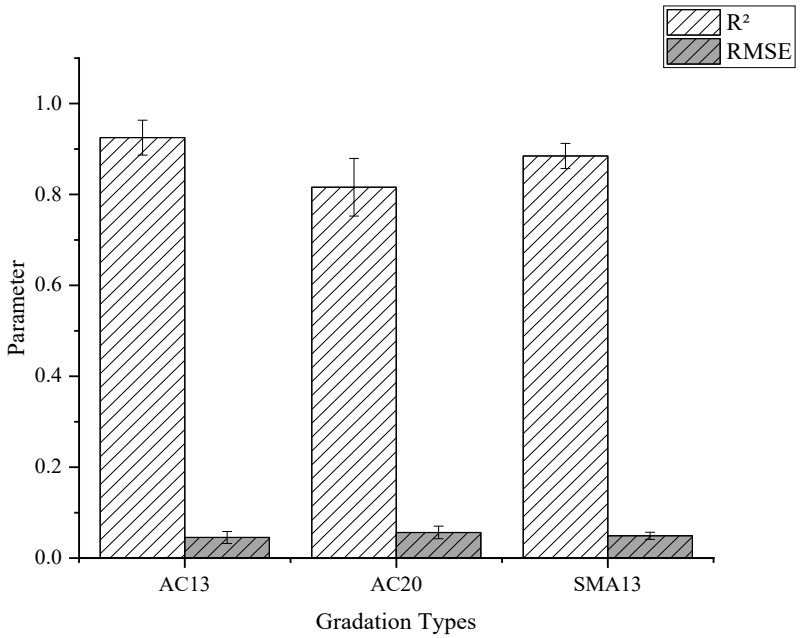

Figure 14. R^2 and RMSE of asphalt pavement with different gradation types.

As a fine-graded asphalt mixture, AC13 gradation uniformly dense surface texture enables parameters such as energy and entropy derived from the GLCM to effectively characterize textural regularity, resulting in the highest model interpretability. In SMA13 gradation, the asphalt mastic thoroughly fills the interstices between coarse aggregates, forming a uniformly embedded structure that reduces textural variability. However, its deeper macro-texture causes a certain degree of RMSE increase from training to testing phases, reflecting minor deviations in the characterization of aggregate interlocking features. For AC20 gradation, the increased proportion of coarse aggregate in this medium-graded mixture leads to non-continuous abrupt changes in surface texture. Parameters including fractal dimension and multifractal spectrum width $\Delta\alpha$ cannot fully quantify such complex textural mutations, causing a substantial increase in testing set RMSE compared to the training set and noticeable attenuation in R^2.

In summary, this model meets high engineering accuracy requirements for asphalt pavements with AC13 and SMA13 gradation types. For applications involving AC20 gradation, the parameter system could be optimized by incorporating coarse texture characteristics.

4.3. Importance analysis of texture features and gradation effect

By analyzing the importance of features, it is possible to reflect the impact of different features on the evaluation results of the model, reveal the degree of dependence of the model on different features, and thus increase the trust and interpretability of the model. To quantify the contribution of different texture

feature parameters to asphalt pavement skid resistance, this study further employed the feature segmentation counting method to investigate the contribution mechanism of various texture features. This method based on the splitting principle of the XGBoost model, quantifies feature importance scores by statistically analyzing the frequency with which each texture feature was selected during decision tree node splitting processes.

As illustrated in Figure 15, the importance ranking of the four features based on full-sample data analysis was: fractal dimension > energy > multifractal spectrum width Δα > entropy. This result indicates that the asphalt pavement anti-skidding performance is primarily governed by the multiscale self-similar characteristics of the texture, which influence pavement skid resistance by characterizing the contact efficiency between aggregate angularity micro-morphology and tires. The macroscopic texture uniformity reflected by energy and the cross-scale roughness fluctuations characterized by multifractal spectrum width Δα synergistically demonstrate their critical role in regulating aggregate distribution patterns. Comparatively, entropy exhibits relatively lower contribution due to its sensitivity to random noise, resulting in slightly insufficient stability within complex pavement surface environments.

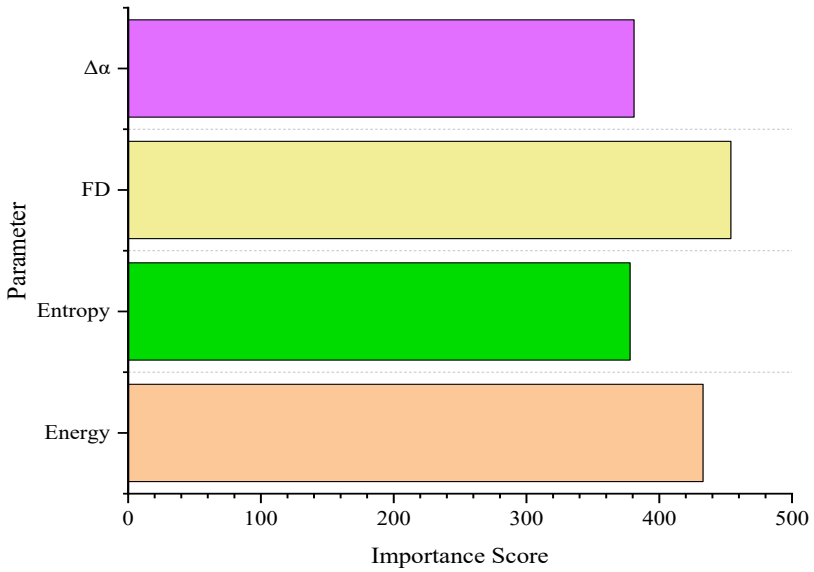

Figure 15. Feature importance ranking (Feature Splitting Counting Method).

As shown in Figure 16 analysis of asphalt pavement data across different gradation types revealed a significant gradation effect. For the AC13 pavement mixture gradation, all feature importance metrics were substantially higher, demonstrating particularly prominent feature sensitivity. This phenomenon originates from the highly continuous texture formed by fine aggregates (nominal particle size ≤ 13 mm), whose uniform structure enables energy to accurately characterize aggregate distribution regularity while fractal models can effectively capture self-similar characteristics of microscopic irregularities. Although SMA13 gradation is similarly classified as fine-graded, asphalt mastic filling causes relative surface smoothing, thereby reducing the importance of both energy and fractal dimension, while the discrete distribution of coarse aggregates within the mastic matrix forms localized mutations, weakening the capacity of the multifractal spectrum width Δα to characterize multiscale features. In AC20 gradation, higher coarse aggregate proportions generate irregular textures exceeding the representational

scope of fractal models, reducing the effectiveness of both fractal dimension and multifractal spectrum width Δα in capturing multiscale characteristics, with discretized aggregate distribution causing grayscale statistical deviations and coarse aggregate interstices inducing random noise interference, collectively lowering the importance of energy and entropy.

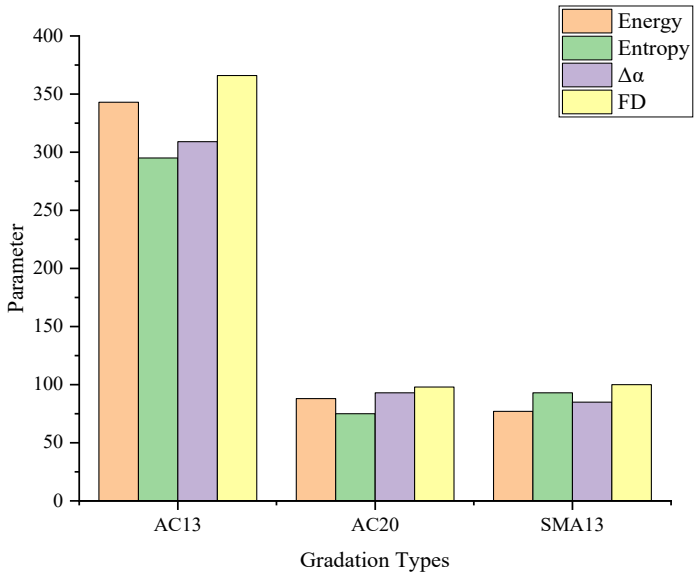

Figure 16. Feature importance ranking of asphalt pavement with different gradation types (Feature Segmentation Counting Method).

Concurrently, differential rankings of texture feature importance among the three gradations reflect the differential control of material structure (gradation type) on the mechanism of texture formation. The uniform distribution of fine aggregates in AC13 gradation forms continuity-dominated surface textures, which increases the importance of energy characterizing macroscopic uniformity and fractal dimension quantifying recursive structures. The filling of SMA13 gradation asphalt mastic changed the texture feature sequence. Although mastic formed a "pseudo-homogeneous background" for filling coarse aggregate gaps, it did not eliminate the local abrupt changes in the edges and corners of the aggregates, amplifying the randomness of its texture and leading to a relative increase in entropy importance. The AC20 gradation reduces the fractal self-similar continuity due to the discrete distribution of coarse aggregates, while forming cross scale roughness changes, making the multifractal spectrum width Δα almost equally dominant with fractal dimension. Aggregate discretization reduces the regularity of grayscale statistics and thereby diminishes energy and entropy importance.

4.4. Verification of anti-skidding performance between evaluation model and field assessment

To verify the feasibility and reliability of the comprehensive skid resistance evaluation model based on the XGBoost algorithm, 60 pavement sections with different gradation types were randomly selected from the Shi-Wu Expressway. The skid resistance evaluation index was calculated using the BPN-specialized XGBoost algorithm. This model was specifically trained with the field-measured British Pendulum Number (BPN) as the prediction target. The same four texture features (Energy, Entropy, Fractal Dimension, and Multifractal Spectrum Width Δα) served as the input variables. By inputting the texture features of the pavement sections into this XGBoost model, it directly outputs the

predicted BPN values. These predicted values were rigorously compared against the BPN values measured on-site using the pendulum friction tester to quantify the correlation between the model evaluation results and the measured BPN values.

As illustrated in Figure 17, the field validation results demonstrated high consistency between the XGBoost model predictions and the actual measured BPN values, with the R^2 exceeding 0.92. Although the RMSE for the BPN-labeled dataset showed an absolute increase compared to that of the texture depth-labeled data, this discrepancy arises from scale dependency due to differences in the magnitude of the target variables. After normalization, the relative error aligned with the accuracy level of the texture depth-labeled data. Together with the high R^2 value, these results confirm the model's applicability in characterizing the friction mechanism.

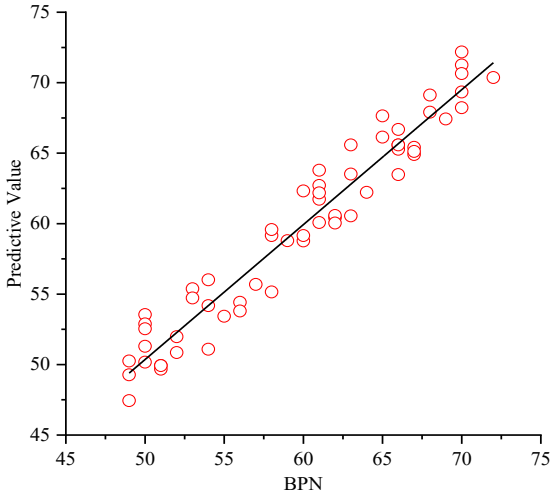

Figure 17. Relationship between model evaluation results and measured BPN.

4.5. Model comparison analysis

To thoroughly evaluate the effectiveness of the XGBoost algorithm in this study and to contextualize its performance within a broader landscape of machine learning algorithms, a comparative analysis was conducted with another widely used ensemble learning algorithm, namely Random Forest (RF). To ensure a fair comparison, both models adopted the same data split (70% for training, 30% for testing) and input features (Energy, Entropy, Fractal Dimension, and Multifractal Spectrum Width $\Delta\alpha$), and their key hyperparameters were optimized using a grid search strategy.

The results in Table 4 indicate that on the identical test set, the Random Forest model also achieved a good performance level ($R^2 = 0.8542$), verifying the fundamental effectiveness of ensemble learning algorithms in solving such complex nonlinear problems. However, the XGBoost model achieved higher predictive accuracy (R^2) and lower error (RMSE) compared to the Random Forest (RF) model. The performance improvement of the XGBoost model is significant. This advantage primarily stems from XGBoost's gradient boosting mechanism and regularization strategy, which enables it to learn more effectively from high-dimensional features and reduce the risk of overfitting. Therefore, these results not only confirm XGBoost's superior capability in capturing the complex nonlinear relationship between pavement texture characteristics and anti-skidding performance but also provide critical support for constructing a precise and reliable evaluation framework for pavement anti-skidding performance.

Table 4. Performance comparison between XGBoost and Random Forest models on the testing set.

Model	R^2	RMSE
XGBoost	0.9322	0.0561
Random Forest	0.8542	0.0688

5. Conclusions

(1) This study constructs a composite parameter-based anti-skidding performance evaluation model using the XGBoost algorithm, achieving prediction accuracy of $R^2 > 0.9$ on the test set, exceeding conventional pavement performance models. The model demonstrates superior accuracy, stability, and robustness by effectively capturing the nonlinear relationships between multi-scale texture features and texture depth (TD).

(2) The model performance exhibits significant gradation-type dependency: AC13 fine-graded mixtures demonstrate optimal prediction accuracy, followed by SMA13, while AC20 showed relatively weaker generalization capability. This gradient originates from the compatibility between material texture characteristics and feature representation. Fractal dimension was identified as the core factor governing skid resistance.

(3) It is important to note that this study was conducted under ideal baseline conditions (dry, clean pavement surfaces). Environmental factors such as water film or dust, which significantly affect texture acquisition in field applications, were not incorporated into the current model. Furthermore, as all data originated from a single expressway, the external validity of the model across different climatic conditions, material variability, and regions needs further verification. Future research will focus on incorporating environmental variables and validating the model with more diverse datasets to enhance its robustness and practical applicability in complex field conditions.

(4) Despite these limitations, the model provides a critical technical pathway for gradation-adaptive anti-skidding evaluation. Future work could focus on integrating morphological parameters for specific gradations and incorporating environmental variables into the model to enhance its practicality and robustness in complex real-world conditions, thereby advancing the maintenance decision-making system for pavements with complex textures toward intelligent and precise iteration.

Acknowledgments

This work is supported by Universiti Sains Malaysia via the Bridging Grant (R501-LR-RND003-0000001344-0000), Key project of Natural Science Research of Anhui Provincial Department of Education (2023AH052853). Research support from the Wuhan Key Research and Development Program (2025050102030009) is also appreciated. Special thanks are extended to the dedicated team of the Sustainable Asphalt Research Group (SARG) at the School of Civil Engineering, USM for their significant assistance throughout this study.

Authors' contribution

Conceptualization, Yu Zhao and Mohd Rosli Mohd Hasan; methodology, Yu Zhao and Mohd Rosli Mohd Hasan; software, Yu Zhao; validation, Yu Zhao, Mohd Rosli Mohd Hasan and Lingyun You; formal analysis, Yu Zhao; investigation, Yu Zhao and Mohd Rosli Mohd Hasan; resources, Mohd Rosli Mohd Hasan; data curation, Yu Zhao and Junxian Jiang; writing—original draft preparation, Yu Zhao; writing—review and editing, Yu Zhao, Mohd Rosli Mohd Hasan, Ke Zhang, Lingyun You, Ali Jamshidi and Junxian Jiang; visualization, Mohd Rosli Mohd Hasan and Ke Zhang; supervision, Mohd Rosli Mohd Hasan; project administration, Mohd Rosli Mohd Hasan; funding acquisition, Mohd Rosli Mohd Hasan and Lingyun You. All authors have read and agreed to the published version of the manuscript.

Conflicts of interests

The authors declare no conflict of interest.

References

[1] Li S, Hu H, Tan Y, Xiao S, Han M, *et al*. A review of non-contact approach for pavement skid resistance evaluation based on texture. *Tribol. Int.* 2024, 196:109737.

[2] Mariani E, Ingrassia LP, Angeloni R, Gorgoglione L, Clini P, *et al*. Interpretation of pavement skid resistance based on the advanced analysis of surface texture. *Transp. Res. Procedia* 2025, 90:495–502.

[3] Zhao W, Zhang J, Lai J, Shi X, Xu Z. Skid resistance of cement concrete pavement in highway tunnel: a review. *Constr. Build. Mater.* 2023. 406:133235.

[4] Guo F, Pei J, Zhang J, Li R, Zhou B, *et al*. Study on the skid resistance of asphalt pavement: a state-of-the-art review and future prospective. *Constr. Build. Mater.* 2021. 303:124411.

[5] Huang X, Zheng B. Research status and prospects of anti-skidding performance for asphalt pavement. *China J. Highway Transp.* 2019. 32(4):32–49.

[6] Fwa TF, Chu L. The concept of pavement skid resistance state. *Road Mater. Pavement Des.* 2021, 22(1):101–120.

[7] Chen Z, Zhang L, Sun D, Xu L, Ni H, *et al*. Skid resistance performance evaluation of semi-flexible pavement based on surface texture features. *Int. J. Pavement Eng.* 2025, 26(1):2520033.

[8] Liu X, Luo H, Chen C, Zhu L, Chen S, *et al*. A technical survey on mechanism and influence factors for asphalt pavement skid-resistance. *Friction* 2024, 12(5):845–868.

[9] Yu M, Chen G, Zhang Z, Li J, Yang L, *et al*. Skid resistance in pavement-vehicle interaction with anti-lock braking systems. *Int. J. Pavement Eng.* 2024, 25(1):2380514.

[10] Plati C, Pomoni M. Impact of traffic volume on pavement macrotexture and skid resistance long-term performance. *Transp. Res. Rec.* 2019, 2673(2):314–322.

[12] Xie T, Yang E, Chen Q, Rao J, Zhang H, *et al*. Separation of macro- and micro-texture to characterize skid resistance of asphalt pavement. *Materials* 2024, 17(20):4961.

[13] Zhang W, Xiao C, Hong Q, Liu J, Yu B, *et al*. Testing and evaluation for skid resistance of steel slag asphalt wearing course based on surface texture characteristics. *Constr. Build. Mater.* 2024, 411:134597.

[14] Yun D, Hu L, Sandberg U, Tang C. Skid resistance performance and texture lateral distribution within the lanes of asphalt pavements. *J. Traffic Transp. Eng.* 2025, 12(1):87–107.
[15] Wang Y, Lai X, Zhou F, Xue J. Evaluation of pavement skid resistance using surface three-dimensional texture data. *Coatings* 2020, 10(2):162.
[16] Do MT, Cerezo V. Road surface texture and skid resistance. *Surf. Topogr. Metrol. Prop.* 2015. 3(4):043001.
[17] Ji J, Jiang T, Ren W, Dong Y, Hou Y, *et al*. Precise characterization of macro-texture and its correlation with anti-skidding performance of pavement. *J. Test. Eval.* 2022, 50(4):1934–1946.
[18] Xie W, Zhang K, Liu Z, Wei G, Zhao Y. Image acquisition method for asphalt pavement based on the characteristic of texture structure. *J. Mater. Sci. Eng.* 2023. 41(4):1673–2812.
[19] Zhang R, Peng B, Zhu Y, Liu H, Zhang Y. A review of modern detection methods for anti-skidding performance of asphalt pavements (In Chinese). *Eng. Mach*. 2024, 55(1):159–164.
[20] Li P, Yi K, Yu H, Xiong J, Xu R. Effect of aggregate properties on long-term skid resistance of asphalt mixture. *J. Mater. Civ. Eng.* 2021, 33(1):04020413.
[21] Meegoda JN, Gao S. Evaluation of pavement skid resistance using high speed texture measurement. *J. Traffic Transp. Eng.* 2015, 2(6):382–390.
[22] Wu J, Wang X, Wang L, Zhang L, Xiao Q, *et al*. Temperature correction and analysis of pavement skid resistance performance based on RIOHTrack full-scale track. *Coatings* 2020, 10(9):832.
[23] Chen Y, Li Z, Wang Y, Liang G, Yang X. A review of long-term skid resistance of asphalt pavement. *Appl. Sci.* 2025, 15(4):1895.
[24] Dan H, Bai G, Zhu Z, Liu X, Cao W. An improved computation method for asphalt pavement texture depth based on multiocular vision 3D reconstruction technology. *Constr. Build. Mater.* 2022, 321:126427.
[24] Dong S, Han S, Zhang Q, Han X, Zhang Z, *et al*. Three-dimensional evaluation method for asphalt pavement texture characteristics. *Constr. Build. Mater.* 2021, 287:122966.
[25] Gupta A, Gowda S, Tiwari A, Gupta AK. XGBoost-SHAP framework for asphalt pavement condition evaluation. *Constr. Build. Mater.* 2024, 426:136182.
[26] Zhao G, Jiang Y, Li S, Tighe S. Exploring implicit relationships between pavement surface friction and vehicle crash severity using interpretable extreme gradient boosting method. *Can. J. Civ. Eng.* 2022, 49(7):1206–1219.
[27] Qin S, Liao W, Huang S, Hu K, Tan Z, *et al*. AIstructure-Copilot: assistant for generative AI-driven intelligent design of building structures. *Smart Constr.* 2024, 1(1):1–20.
[28] Wu Y. From ensemble learning to deep ensemble learning: a case study on multi-indicator prediction of pavement performance. *Appl. Soft Comput.* 2024, 166:112188.
[29] Zhang K, Sun P, Li L, Zhao Y, Zhao Y, *et al*. A novel evaluation method of aggregate distribution homogeneity for asphalt pavement based on the characteristics of texture structure. *Constr. Build. Mater.* 2021, 306:124927.
[30] Zhao X, Xue L, Xu F. Asphalt pavement paving segregation detection method using more efficiency and quality texture features extract algorithm. *Constr. Build. Mater.* 2021, 277:122302.
[31] He J, Shao L, Li Y, Wang K, Liu W. Pavement damage identification and evaluation in UAV-captured images using gray level co-occurrence matrix and cloud model. *J. King Saud Univ.-Comput. Inf. Sci.* 2023, 35(9):101762.

[32] Chen D. Evaluating asphalt pavement surface texture using 3D digital imaging. *Int. J. Pavement Eng.* 2020, 21(4):416–427.
[33] Zhang K, Xi D, Zhao Y, Xie W, Zhang W, *et al*. Research on the skidding resistance and attenuation characteristics of asphalt pavement based on image recognition-analysis strategy. *Coatings* 2024, 14(6):749.
[34] Aouat S, Ait-Hammi I, Hamouchene I. A new approach for texture segmentation based on the gray level co-occurrence matrix. *Multimedia Tools Appl.* 2021, 80(16):24027–24052.
[35] Alfwzan WF, Alballa T, Al-Dayel IA, Selim MM. Asphalt pavement patch identification with image features based on statistical properties using machine learning. *Neural Comput. Appl.* 2024, 36(17):10123–10141.
[36] Ahammed MA, Tighe SL. Early-life, long-term, and seasonal variations in skid resistance in flexible and rigid pavements. *Transp. Res. Rec.* 2009, 2094(1):112–120.
[37] Suresh A, Shunmuganathan K. Image texture classification using gray level co-occurrence matrix based statistical features. *Eur. J. Sci. Res.* 2012, 75(4):591–597.
[38] Luo Y, Xu Y, Li Y, Wang L, Wang H. The effective depth of skid resistance (EDSR): a novel approach to detecting skid resistance in asphalt pavements. *Materials* 2025, 18(6):1204.
[39] Matlack GR, Horn A, Aldo A, Walubita LF, Naik B, *et al*. Measuring surface texture of in-service asphalt pavement: evaluation of two proposed hand-portable methods. *Road Mater. Pavement Des.* 2023, 24(2):592–608.
[40] Zhang K, Wei G, Luo Y, Zhao Y, Zhao Y, *et al*. Evaluation of aggregate distribution homogeneity for asphalt pavement based on the fractal characteristic of three-dimensional texture. *Int. J. Pavement Res. Technol.* 2024, 17(3):577–594.
[41] Bouzeboudja H, Melbouci B, Bouzeboudja A. Experimental study of crushed granular materials by the notion of fractal dimension in 2D and 3D. *Geotech. Geol. Eng.* 2022, 40(4):2009–2031.
[42] Ren Z, Tan Y, Huang L, Xiao S. Fractal and multifractal characteristics of three-dimensional meso-structure for asphalt mixture. *Constr. Build. Mater.* 2023, 384:131429.
[43] Chen S, Liu X, Luo H, Yu J, Chen F, *et al*. A state-of-the-art review of asphalt pavement surface texture and its measurement techniques. *J. Road Eng.* 2022, 2(2):156–180.
[44] Costa VG, Pedreira CE. Recent advances in decision trees: an updated survey. *Artif. Intell. Rev.* 2023, 56(5):4765–4800.
[45] Bansal M, Goyal A, Choudhary A. A comparative analysis of K-nearest neighbor, genetic, support vector machine, decision tree, and long short term memory algorithms in machine learning. *Decis. Anal. J.* 2022, 3:100071.
[46] Yang Y, Lv H, Chen N. A Survey on ensemble learning under the era of deep learning. *Artif. Intell. Rev.* 2023, 56(6):5545–5589.
[47] Jiang S, Li Z, Zhang R, Zheng J, Zhou S. A back-analysis method of deep excavation in soft soil based on BIM-NS-ML integrated technology. *Smart Constr.* 2025, 2(1):1–18.
[48] Zhou Z. *Machine learning*, 1st ed. Singapore: Springer nature, 2021.
[48] Matloob F, Ghazal TM, Taleb N, Aftab S, *et al*. Software defect prediction using ensemble learning: a systematic literature review. *IEEE Access* 2021, 9:98754–98771.
[50] Hakkal S, Lahcen AA. XGBoost To enhance learner performance prediction. *Comput. Educ.: Artif. Intell.* 2024, 7:100254.

[51] Gong H, Sun Y, Shu X, Huang B. Use of random forests regression for predicting IRI of asphalt pavements. *Constr. Build. Mater.* 2018, 189:890–897.

[52] Kong F, Ma Y, Xu B, Lu D, Du X. Dual-driven prediction on stratum displacement induced by shield tunnel excavation based on machine learning and analytical methods. *Smart Constr.* 2025. 2(4):1–21.

[53] Chen Y, Yang X, Lin J, Xie G, Zhang M, *et al*. Predicting bond-slip behaviour in grouted bellows connect rebar using deep learning. *Smart Constr.* 2025, 2(1):1–27.